Chemical Engineering Journal 156 (2010) 582–587

Contents lists available at ScienceDirect

Chemical Engineering Journal

journal homepage: www.elsevier.com/locate/cej

Computational fluid dynamic simulation of fluid flow in a rotating packed bed

Wenjing Yang[a], Yundong Wang[a,*], Jianfeng Chen[b], Weiyang Fei[a]

[a] The State Key Laboratory of Chemical Engineering, Department of Chemical Engineering, Tsinghua University, Beijing 100084, PR China
[b] Research Center of the Ministry of Education for High Gravity Engineering and Technology, College of Chemical Engineering, Beijing University of Chemical Technology, Beijing 100029, PR China

ARTICLE INFO

Article history:
Received 5 November 2008
Received in revised form 24 February 2009
Accepted 2 April 2009

Keywords:
Rotating packed bed (RPB)
Mass-transfer
Fluid dynamics
Simulation
Pressure drop

ABSTRACT

Rotating packed bed (RPB) has been widely used in absorption, desorption, distillation, oxidation, crystallization, precipitation, polymerization, and production of nanoparticles. RPB utilizes centrifugal acceleration to intensify the mixing and mass-transfer processes. Under high-gravity, molecule diffusions are much faster than under normal gravity. With the centrifugal force generated by rotation, RPBs have considerable high mass-transfer and micromixing performance. However, because of the complexity of fluid flow inside the RPB, the flow experiments do not easily lead to the deeper understanding on the fluid dynamics in an RPB. In this paper, computational fluid dynamics model and two-, three-dimensional physical models have been developed to describe the RPB. Numerical simulation of the fluid flow and pressure drop in dry bed in an RPB using commercial software, Fluent, as a computational platform has been carried out. Different fluid flow rates, rotator speeds and gas flow rates have been systematically investigated. The preliminary simulation results show that the models used to describe the RPB can give rise to better understanding of the flow in an RPB.

1. Introduction

Since the first rotating packed bed (RPB) was introduced in the 1970s, it has been widely used in absorption, desorption, distillation, oxidation, crystallization, precipitation, polymerization, and production of nanoparticles, then there has been an industrial drive for researches on the RPB. The essence of RPB is to produce a high gravitational environment by a centrifugal force. The rotating packed bed as the process intensified device is becoming popular in industry [1–5].

While most of the published studies of the RPB were focused on its applications, the fundamental researches are relatively insufficient, for the fluid flow inside the RPB is complex and the flow experiments do not easily lead to the deeper understanding on the fluid dynamics in an RPB.

Burns and Ramshaw [6] took the visual study of liquid flow in RPBs under the rotating speed that ranged from 300 r/min to 1000 r/min. They observed the spiral of liquid and severe liquid maldistribution on radial orientation, in contrast the liquid wandered slightly laterally and consequently led to a relatively uniform distribution on the tangential orientation. Similar results were reached by the researchers [7] in Beijing University of Chemical Technology. Unfortunately still there are no precise experimental data about the flow in RPBs. With the fast development of the computer technology, CFD can predict the fluid flow where the experimental methods cannot work. Because the packings in the RPB are geometrical complex, the reports on the simulation of the fluid flow in the RPB are in scarcity. Our present work aims at a contribution to reliable numerical predictions of the fluid in the RPB. We developed a computational fluid dynamics model and two-, and three-dimensional physical model to describe the rotating packed bed. Numerical simulation of the fluid flow and pressure drop (dry bed) in an RPB using commercial software, Fluent, as a computational platform, has been carried out. Different fluid flow rates, rotator speeds and gas flow rates have been systematically investigated. The preliminary simulation results show that the models to describe the RPB can give rise to better understanding of the flow in an RPB.

2. Model

2.1. Description of the physical model development

The RPB consists of a rotating packed bed in the shape of a torus. Liquid is sprayed on from the distributor in the inside edge of the packed bed and is thrown outwards by the centrifugal force. Gas is introduced from the outside and, due to the imposed pressure gradient, flows inward to the liquid (Fig. 1) [4,5]. The wire mesh packing is very common in the RPBs. In our work, some assumptions are used to simplify the mesh packings. First, the wires are all

* Corresponding author.
E-mail address: wangyd@tsinghua.edu.cn (Y. Wang).

1385-8947/$ – see front matter © 2009 Elsevier B.V. All rights reserved.
doi:10.1016/j.cej.2009.04.013

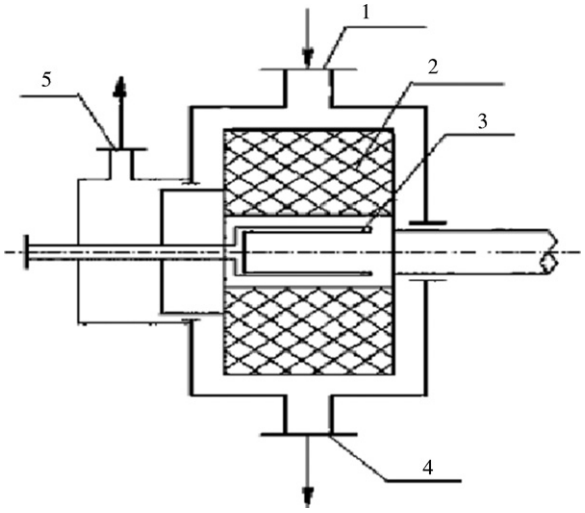

Fig. 1. Schematic diagram of RPB. (1) Gas inlet, (2) packing, (3) distributor, (4) liquid outlet, (5) gas outlet.

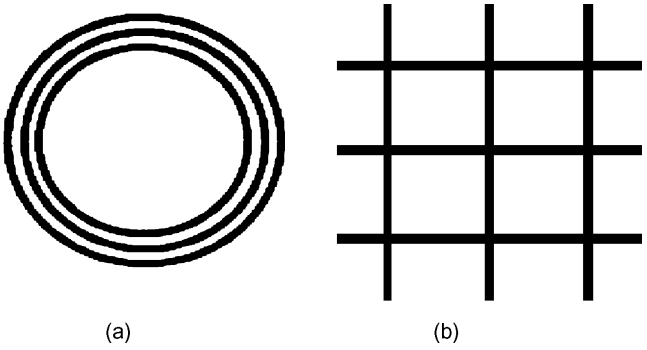

Fig. 2. Schematic diagram of wire mesh arrangement (a) and simplification(b).

0.5 mm thick. Second, the holes of the mesh are strictly square holes (5 mm × 5 mm). Third, the single meshes are arranged in the shape of a torus (Fig. 2(a)), and the space between two neighbor meshes is 1 mm wide (Fig. 2(b)). In our 2D physical model, the mesh packing seem like the foursquare obstacles, and they are arranged in circle to simulate the single mesh while in radial to simulate the meshes in the shape of a torus (Figs. 3 and 4). Figs. 5 and 6 show the 3D model we developed. Unlike the 2D ones, the packing thickness in this model is only 20 mm, for meeting the high request of the computer's capacity.

2.2. Computational grid

A commercial software Fluent 6.2.16 combined with Gambit 2.2.30 was used in the present study. FLUENT provides complete

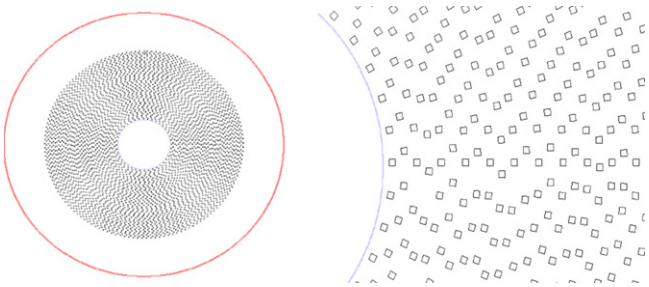

Fig. 3. 2D physical model of the RPB and the packing.

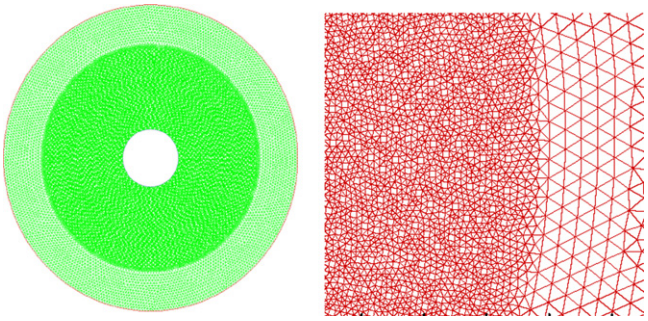

Fig. 4. Unstructured grid of 2D model.

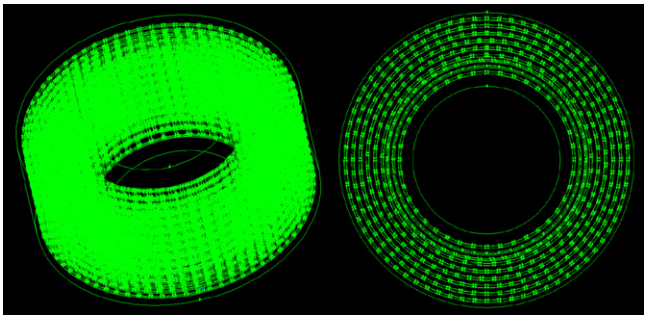

Fig. 5. 3D physical model of the RPB and the packing.

mesh flexibility, including the ability to solve flow problems using unstructured meshes that can generate the complex geometries with relative ease. Supported mesh types include 2D triangular quadrilateral, 3D tetrahedral/hexahedral/pyramid/wedge, and mixed (hybrid) meshes. This architecture allows for efficient execution, interactive control, and complete flexibility between different types of machines or operating systems. All functions required to compute a solution and display the results are accessible in FLUENT through an interactive, menu driven interface.

The 2D computational grid shown in Fig. 4, an unstructured grid, consists of 99,844 triangular mesh elements. To resolve the highly nonuniform flow field in the vicinity of the packing zone, the grid was locally refined with 91,292 mesh elements. And in the zone without packing only the coarse grid was created to save the cost of the computer. The ratio between the coarse grid and fined grid is approximately 6. To 3D model, as shown in Fig. 6, the tetrahedral and pyramid mesh elements, which has 1,071,338 and 26,190 respectively, form the 3D computational grid. And more than 90% 3D mesh elements are in the range of 0.1–0.6 mm^2.

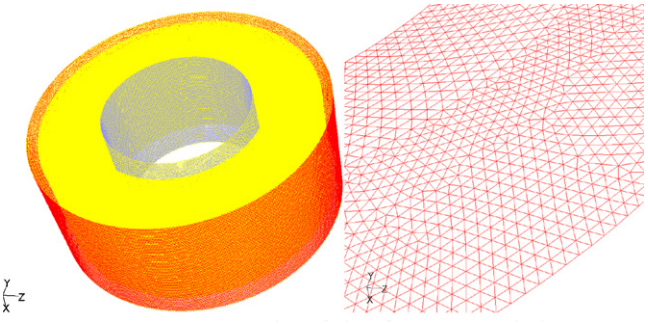

Fig. 6. Unstructured grid of 3D model.

Table 1
Specification of the RPB used in this study.

Rotor	Inner radius = 30 mm	Outer radius = 160 mm	Axial height = 50 mm
Packing	Wire mesh		

2.3. CFD theory

Based on the physical model, a single-phase fluid flow in the RPB was simulated. The medium is pure water, and there is no temperature gradient, so only the mass conservation and the momentum equations are used.

$$\text{Mass conservation}: \quad \frac{\partial \rho}{\partial t} + \text{div}(\rho V) = 0 \tag{1}$$

x-momentum equation :

$$\frac{\partial(\rho u)}{\partial t}\text{div}(\rho u V) = -\frac{\partial p}{\partial x} + \text{div}(\mu\ \text{grad}\ u) S_{Mx} \tag{2}$$

y-momentum equation :

$$\frac{\partial(\rho v)}{\partial t}\text{div}(\rho v V) = -\frac{\partial p}{\partial y} + \text{div}(\mu\ \text{grad}\ v) S_{My} \tag{3}$$

z-momentum equation :

$$\frac{\partial(\rho w)}{\partial t}\text{div}(\rho w V) = -\frac{\partial p}{\partial z} + \text{div}(\mu\ \text{grad}\ w) S_{Mz} \tag{4}$$

The realizable $k-\varepsilon$ model has been extensively validated for a wide range of flows, including rotating homogeneous shear flows, free flows including jets and mixing layers, channel and boundary layer flows, and separated flows. For all these cases, the performance of the model has been found to be substantially better than that of the standard $k-\varepsilon$ model. The term "realizable" means that the model satisfies certain mathematical constraints on the normal stresses, consistent with the physics of turbulent flows. The turbulence kinetic energy, k, and its rate of dissipation, ε, are obtained from the following transport equations:

$$\frac{\partial}{\partial t}(\rho k) + \frac{\partial}{\partial x_i}(\rho k u_i) = \frac{\partial}{\partial x_i}\left[\left(\mu + \frac{\mu_t}{\sigma_k}\right)\frac{\partial k}{\partial x_j}\right] + G_k + G_b - \rho\varepsilon - Y_M + S_k \tag{5}$$

$$\frac{\partial}{\partial t}(\rho \varepsilon) + \frac{\partial}{\partial x_i}(\rho \varepsilon u_i) = \frac{\partial}{\partial x_i}\left[\left(\mu + \frac{\mu_t}{\sigma_\varepsilon}\right)\frac{\partial \varepsilon}{\partial x_j}\right] + \rho C_1 S\varepsilon - \rho C_2 \frac{\varepsilon^2}{k + \sqrt{\nu\varepsilon}} + C_{1\varepsilon}\frac{\varepsilon}{k}(C_{3\varepsilon}G_b + S_\varepsilon) \tag{6}$$

where G_k is the generation of turbulence kinetic energy due to the mean velocity gradients, G_b the generation of turbulence kinetic energy due to buoyancy, Y_M the contribution of the fluctuating dilatation in compressible turbulence to the overall dissipation rate, C_2 and $C_{1\varepsilon}$ are constants, σ_k and σ_ε are the turbulent Prandtl numbers for k and ε, S_k and S_ε user-defined source terms. The turbulent viscosity, μ_t, is computed by combining k and ε as follows:

$$\mu_t + \rho C_\mu \frac{k^2}{\varepsilon} \tag{7}$$

$$C_\mu = \frac{1}{A_0 + A_s k U^*/\varepsilon} \tag{8}$$

$$U^* \equiv \sqrt{S_{ij}S_{ij} + \tilde{\Omega} i_j \tilde{\Omega}_{ij}} \tag{9}$$

where $\tilde{\Omega}_{ij}$ is the mean rate-of-rotation tensor viewed in a rotating reference frame with the angular velocity ω_k The model constants A_0 and A_s are given by

$$A_0 = 4.04, \quad A_s = \sqrt{6}\cos\phi$$

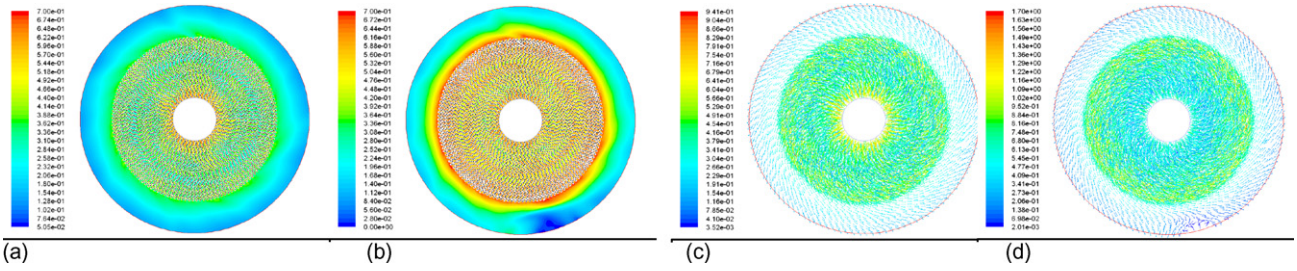

Fig. 7. The velocity contours and vectors at the inlet velocity of 0.5 m/s.

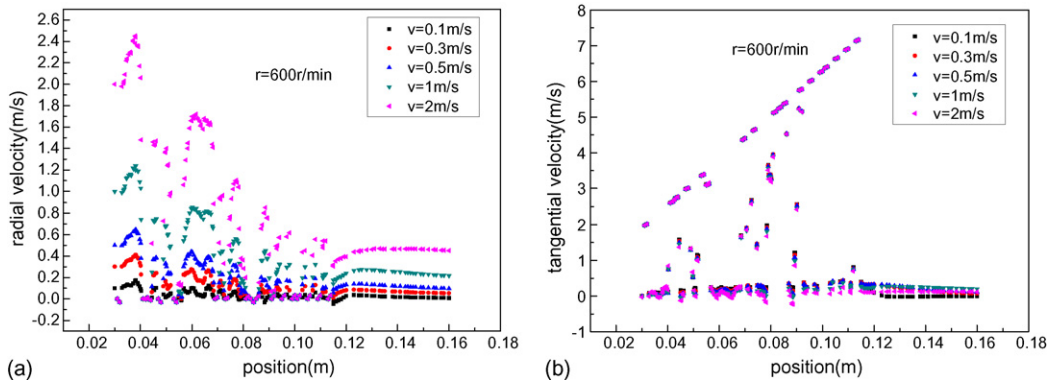

Fig. 8. Effect of inlet velocity on velocity distribution along the radial direction.

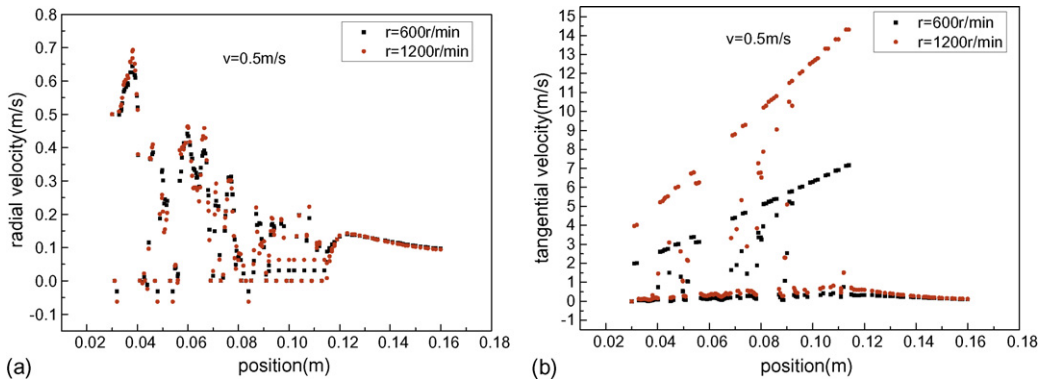

Fig. 9. Effect of rotator speed on velocity distribution along the radial direction.

The model constants have the following default values:

$$C_{1\varepsilon} = 1.44; \quad C_{2\varepsilon} - 1.92; \quad C_{\mu} = 0.09; \quad \sigma_k = 1.0; \quad \sigma_{\varepsilon} = 1.3$$

In this study, the fluid flows with different inlet velocities (0.3–10 m/s) and different rotational speeds (400–1200 r/min) were performed. Table 1 shows the size of the RPB simulated. The wire mesh packing's pore size is on the order of 5 mm. The inner and outer diameters are 30 mm and 160 mm respectively, and the axial height is 50 mm.

The inlet velocities were specified at the inlet boundary condition. All the surfaces of the packing were defined as moving walls to get the aimed centrifugal force. The simulation was run until the nondimensional residuals of the continuity, turbulence kinetic energy (k), its dissipation rate (ε) and x, y velocity decayed by three orders of magnitudes (0.0001). The computations of 2D model were run on a 1.87 GHz computer with 2048 MB random access memory, while the 3D one on a high performance computing server which has 2× QuadCore Intel Xeon X5355, 2666 MHz (8 × 333), random access memory: 8192 MB.

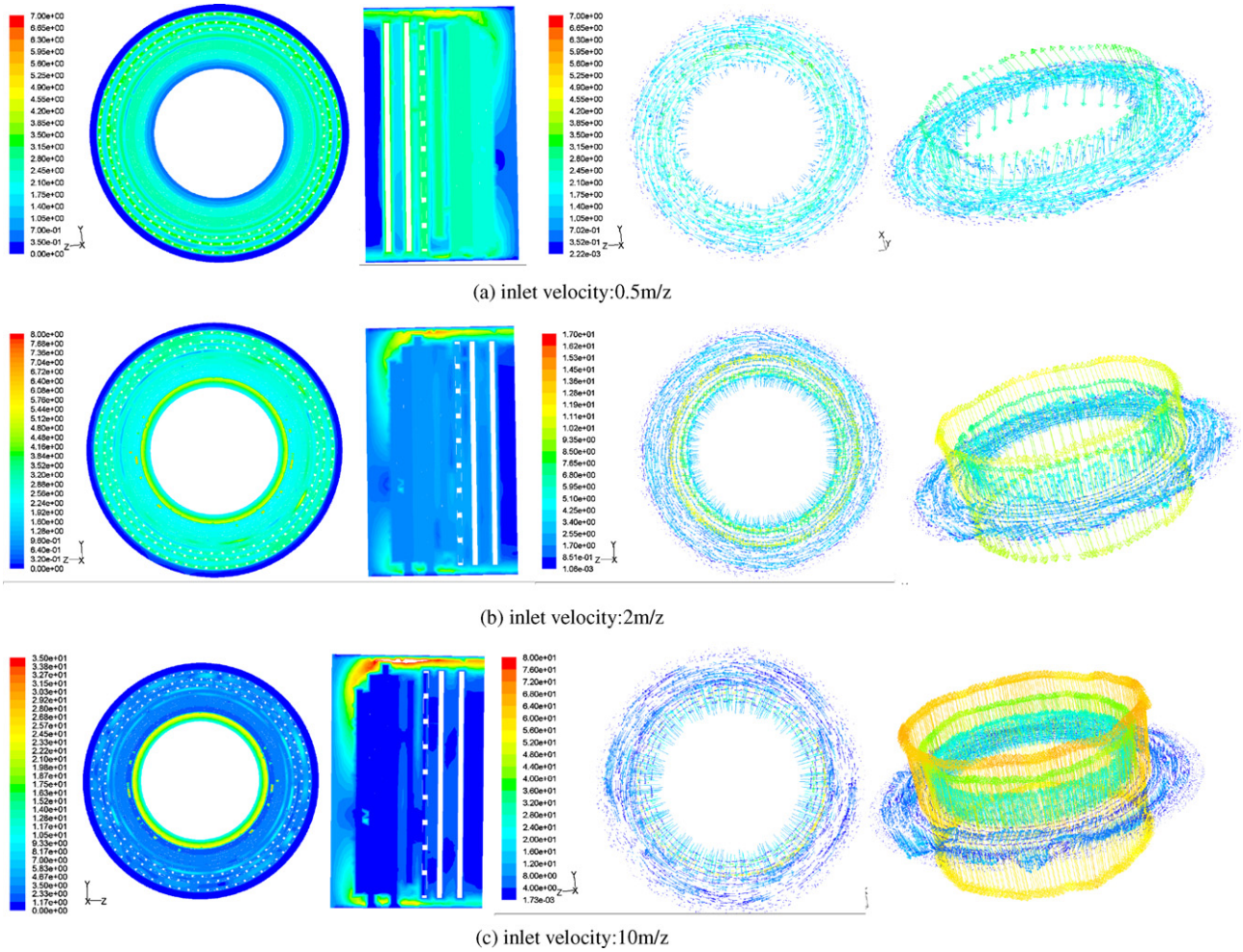

(a) inlet velocity:0.5m/z

(b) inlet velocity:2m/z

(c) inlet velocity:10m/z

Fig. 10. The velocity contours (x-section and y-section) and vectors at rotational speed of 600 r/min.

3. Results and discussion

3.1. Fluid flow

3.1.1. 2D model

Fig. 7 shows velocity contours and vectors at the inlet velocity of 0.5 m/s. As the figure indicates, the fluid flow is heavily influenced by the packing's rotation, and the same phenomena can be seen while the velocities are lower than 2 m/s, but while $v < 0.2$ m/s, the realizable $k-\varepsilon$ model can not reflect the flow correctly, and the laminar model should be used. However, with the inlet velocities (>2 m/s) the flow is less affected by the packing's rotation, and the flow is mainly on the radial direction. For the size of the RPB we simulated, the inlet velocity (0.2–1 m/s) is a proper magnitude of the inlet velocity. Fig. 7 also reveals that the higher rotational speed leads to the stronger tangential flow and a more even velocity distribution.

Fig. 8 illustrates the distributions of the velocity along the radial and tangential direction versus inlet velocities (0.1–2 m/s) on the rotational speeds, 600 r/min. The radial velocity plots are a family of curves with the intercepts on the ordinate increasing with an increase in inlet velocity. In the packing zone (0.035–0.11 m), the radial velocities are fluctuant but the overall trend diminishes along the radial direction. In the no-packing zone (0.11–0.16 m) the radial velocities are almost steady and nearly parallel to each other. On the other side, under all the inlet velocities we investigated, the tangential velocity plots are almost identical.

In Fig. 9, the effects of rotation speeds on radial and tangential velocity distributions are shown. Under 600 r/min and 1200 r/min, the radial velocities are the same. However under 1200 r/min, the tangential velocity plot is much higher than the one under 600 r/min, moreover a larger slop is also obvious under 1200 r/min.

In total, it is evident that the radial velocity is sensitive to the inlet velocity, but isn't influenced by the rotation speeds, while to the tangential velocity, the packing rotation is the key factor to its distribution.

3.1.2. 3D model

In the results of 3D model, Fig. 10, from the x-section contours and vectors we easily find that the axial velocity is too low to have influence on the fluid flow in the main packing zone. However from the last column of vectors in a 3D view, we could clearly see a sharp increase of axial velocity in the inlet zone. And this phenomenon is enhanced by inlet velocity's growth and nearly has no relation to the rotator speed. By comparing the tangential velocity along the radial orientation under different rotator speed, from 400 r/min to 1200 r/min, as shown in Fig. 11, despite of the same results as 2D model, we still reach some new points, like the lower velocity zone behind the packing, and the degree of this decrease is inclined with the rotator speed increase. In other researchers' work, this phenomenon can be deduced from the pressure drop in the wet bed as a reason to explain the lower pressure drop in wet bed than in dry bed [9].

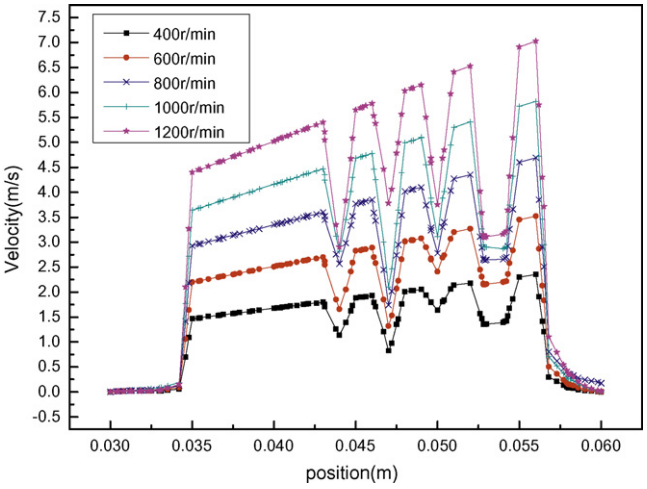

Fig. 11. The distributions of the tangential velocity under different rotator speed.

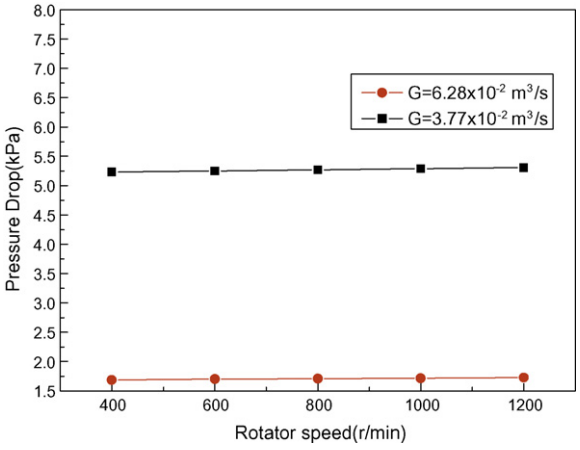

Fig. 12. Effect of rotor speed on pressure drop.

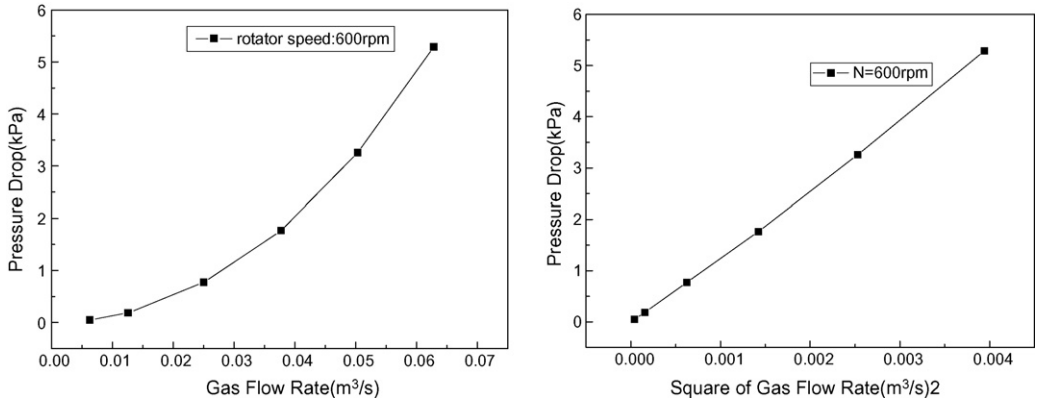

Fig. 13. Effect of gas flow rate on pressure drop.

3.2. The pressure drop in dry bed

Besides the fluid flow, we also considered the RPB's pressure drop in dry bed, which has been investigated extensively by previous experiments [8–10]. The effect of the rotor speed on the pressure drop is shown in Fig. 12 when there is no liquid in the rotor, namely dry bed. It implies the pressure drop linearly varies with the rotor speed at a rather low slope, almost equal to 0, which can easily lead to the conclusion: the rotor speed has little effect on the pressure drop. From the experimental work of Zheng and co-workers [10], the similar results are unfolded, that is compared to gas flow rate the rotator speed has much less influence on pressure drop in dry bed. But actually in spite of the discrepancy in the size of the beds, the simulated data (about 10–50 Pa) are much lower than the experimental (about 100–1000 Pa) in magnitude. The cause of this phenomenon may be owing to the inlet and outlet tube pressure drop that are ignored in our simulation.

As Fig. 13 shows, the overall pressure drop is investigated versus gas flow rate at a constant rotor speed, that is 600 r/min, and the range of gas flow rate is from 0.006 m^3/s to 0.07 m^3/s. From the simulated data, the same conclusion as the previous experiments [10] is obvious: the pressure drop is strongly dependent on the gas flow rate, and linear with the square of gas flow rate.

4. Conclusions

Previously reported studies of RPB are almost about the applications, and the fundamental researches are not sufficient at all. This paper presented a 2D and 3D model to predict the fluid flow in the RPB, and the simulations of monophase flow are reasonable and can reflect the features of the flow in the RPB. Moreover, the pressure drop in a dry bed calculated by us is consistent with the data in experiments, so the model we developed can reflect the fluid and gas flow in an RPB correctly to some extent. Therefore, with our CFD model, more simulations of the monophase, such as micromixing efficiency, can be taken out to lead more useful work about the fundamental researches.

Acknowledgements

This research was carried out under the National High Technology Research and Development Programmes of China (No. 2006AA05Z316 and No. 2006AA030202) and the Specialised Research Fund for Doctoral Programme of Higher Education of China (No. 20070003154) in the State Key Laboratory of Chemical Engineering of Tsinghua University, Beijing, PR China. The authors gratefully acknowledge these grants.

References

[1] Jianfeng Chen, Technology and Application of High Gravity, Chemical Industry Press, Beijing, China, 2003 (in Chinese).
[2] C. Ramshaw, Higee distillation-an example of process intensification, Chem. Eng. 90 (1983) 13–14.
[3] T. Kelleher, J.R. Fair, Distillation studies in a high-gravity contactor, Ind. Eng. Chem. Res. 35 (1996) 4646–4655.
[4] S. Munjal, M.P. Dudukovic, P. Ramachandran, Mass-transfer in rotating packed beds: development of gas-liquid and liquid-solid mass-transfer correlations, Chem. Eng. Sci. 44 (1989) 2245–2256.
[5] S. Munjal, M.P. Dudukovic, P. Ramachandran, Mass-transfer in rotating packed beds: experimental results and comparison with theory and gravity flow, Chem. Eng. Sci. 44 (1989) 2257–2268.
[6] J.R. Burns, C. Ramshaw, Process intensifications: visual study of liquid maldistribution in rotating beds, Chem. Eng. Sci. 51 (1996) 1347–1352.
[7] Kai Guo, Fen Guo, Yuanding Feng, Jianfeng Chen, Chong Zheng, Nelson C. Gatdner, Synchronous visual and RTD study on liquid flow in rotating packed-bed contactor, Chem. Eng. Sci. 55 (2000) 1699–1706.
[8] Hwai-Shen Liu, Chia-Chang Lin, Characteristics of a rotating packed bed, Ind. Eng. Chem. Res. 35 (1996) 3590–3596.
[9] Zhenhu Li, Kai Guo, Research into characteristic of gas pressure drop pf a rotating packed bed, J. Beijing Univ. Chem. Technol. 26 (1999) 5–10 (in chinese).
[10] Chong Zheng, Kai Guo, Yuanding Feng, Cun Yang, Pressure drop of centripetal gas flow through rotating bed, Ind. Eng. Chem. Res. 39 (2000) 829–834.